Flux ratios of primary elements measured by CALET on the International Space Station

Caterina Checchia,[a,b,*] **Francesco Stolzi**[a,b] **for the CALET collaboration**

[a]*Department of Physical Sciences, Earth and Environment,*
University of Siena, via Roma 56, 53100 Siena, Italy

[b]*INFN Sezione di Pisa,*
Polo Fibonacci, Largo B. Pontecorvo, 3, 56127 Pisa, Italy

E-mail: caterina.checchia2@unisi.it, francesco.stolzi@unisi.it

The study of flux ratios of cosmic-ray primary elements is of particular interest not only to assess the relative abundance of each element, but also to gain a deeper understanding of their propagation in the galaxy. High energy cosmic ray data are the best candidate for this purpose as convection, nuclear decay, and energy degradation can be neglected during their propagation. CALET on the International Space Station has been measuring the flux of several primary elements from proton to nickel for 7 years to date. In this contribution, the flux ratios of heavy primary elements to lighter primaries will be shown, extending the energy range already investigated by previous measurements.

38th International Cosmic Ray Conference (ICRC2023)
26 July - 3 August, 2023
Nagoya, Japan

ICRC2023
38th International Cosmic Ray Conference
The Astroparticle Physics Conference

---

*Speaker

1. Introduction

Primary cosmic rays are thought to be mainly produced and accelerated in astrophysical sources. The study of their flux ratios provides important information on the origin, acceleration, and propagation processes of cosmic rays in the Galaxy. At the time of writing most of the measurements of primary flux ratios are concentrated at energies below a few GeV/n. Beyond this energy, the CREAM-II [1] confirms, up to 800 GeV/n, the nearly flat trend of HEAO3–C2 [2] low-energy data for Ne/O and Mg/O ratios while revealed that Si/O and Fe/O ratios seem to increase with energy. The AMS results revealed differences in the rigidity dependence of the Ne, Mg and Si fluxes compared to the He, C, O and Fe fluxes [3–6], while CALET [7] confirmed the same energy dependence for C and O fluxes. Few measurements appear concerning nickel ratios also at low energy [2, 8–10]. The Calorimetric Electron Telescope (CALET) [11–14] is a space-based instrument optimized for the measurement of the all-electron spectrum [15, 16], which can also measure individual chemical elements in CR and their ratio from proton to nickel in the energy range up to $\sim$ 1 PeV [7, 17–21]. In this contribution, we report the Fe/He, Fe/O, Fe/C, Ni/He, Ni/O, Ni/C, O/He, C/He, O/C and Ni/Fe flux ratios based on the data collected by CALET from November 1, 2015 to December 31, 2022 aboard the International Space Station (ISS).

2. CALET Instrument

CALET consists of a charge detector (CHD), a finely segmented imaging calorimeter (IMC) and a total absorption calorimeter (TASC). The CHD consists of two hodoscopes, each equipped with 14 plastic scintillator paddles arranged in orthogonal layers (CHDX, CHDY). The CHD is capable of resolving individual chemical elements from Z = 1 up to Z = 40 with excellent charge resolution. The IMC also provides an independent measurement of the charge by multiple sampling of the specific energy loss (dE/dx) in each fiber up to the onset of saturation, which occurs for ions more highly charged than silicon. The IMC, which consists of 16 layers of thin scintillating fibers that are readout individually, reconstructs the direction of the CR particles. The TASC is a homogeneous calorimeter consisting of lead tungstate (PWO) bars arranged in 12 layers. The crystal bars in the top layers are read by photomultiplier tubes. In the remaining layers, a dual photodiode-avalanche-photodiode (PD-APD) system is used for each channel. Using front-end electronics with dual gain ranges for each photosensor, a dynamic range of more than 6 orders of magnitude is covered. The total thickness of the instrument is equivalent to 30 radiation lengths and 1.3 proton interaction lengths. Monte Carlo (MC) simulations, based on the EPICS simulation package [22], were used to reproduce the detailed detector configuration, physical processes, as well as detector signals and to evaluate event reconstruction efficiencies, background contamination and the energy response matrix. Independent simulations based on FLUKA [23, 24] and GEANT4 [25] are used to evaluate the systematic uncertainties. The instrument was launched on August 19, 2015 and it was placed on the Japanese Experiment Module Exposed Facility (JEM EF) on the ISS. Scientific observations began on October 13, 2015 [26]. Since then, the instrument has been in smooth and continuous operation.

3. Data Analysis

The flux ratios reported here use the C, O, Fe and Ni fluxes updated with respect to our previous publication [7, 19–21], extending the collected statistics to 2618 days, and the helium flux as published in [18] for a total of 2392 days of data collection. The total observation live time for the high-energy (HE) shower trigger is $T \sim 5.3 \times 10^4$ h, corresponding to $\sim 86.\%$ of total observation time (4.8×10^4 h for helium flux). The raw data are corrected for the non-uniformity of the light output, for the time and temperature dependence and for the gain differences between the channels. The latter are individually calibrated on orbit using penetrating proton and He particles. These are selected by a special trigger mode [27]. After calibration, we reconstructed a track for each CR particle, and each event is associated with an estimate of its charge and energy. A tracking algorithm, based on a combinatorial Kalman filter, uses the information provided by the coordinates of the scintillating fibers in the IMC to find and fit the track of the incident particle. All reconstructed events with one well-fitted track passing through the top surface of the CHD and the bottom surface of the TASC (excluding a border region of 2 cm) are then selected. The geometrical acceptance for this category of events is $S\Omega \sim 510 \, cm^2 sr$. Light nuclei candidates are searched for among events selected by the onboard high-energy (HE) shower trigger, which requires the coincidence of the summed signals of the last two IMC double layers and the top TASC layer. Consistency between MC and FD for triggered events is obtained by an off-line trigger with higher threshold than the onboard trigger. Since the HE trigger is fully efficient (close to 100%) for elements heavier than oxygen, the selection of interacting particles requires a deposit larger (by 2 sigmas) than the minimum ionization particle (MIP) peak in at least one of the first four TASC layers (shower event cut). The identification of the particle charge Z is based on the measurements of the ionization deposits in CHD and IMC. Three independent *dE/dx* measurements are obtained, one for each CHD layer and the third by averaging the samples along the track in the IMC. These measurements are corrected for the quenching effect in the scintillator's light yield. For nuclei with Z greater than silicon, only the CHD is used due to the saturation of signals occurring in the upstream IMC layers. The identification of each candidate nucleus differs between light and heavy nuclei and is explained in detail in the following references [7, 18–21]. The background contamination in the final nucleus sample is estimated from MC distributions in different intervals of $E_{T\,ASC}$, after applying the complete charge selection procedure.

The shower energy $E_{T\,ASC}$ of each event is calculated as the sum of the energy deposits of all TASC logs after stitching the adjacent gain ranges of each PD-APD [28]. The TASC response was studied at CERN SPS in 2015 using a beam of accelerated ion fragments with A/Z = 2, obtained with a primary beam of ^{40}Ar nuclei, and kinetic energy of 13, 19 and 150 GeV/*c*/*n* [29]. The energy response was found to be linear up to the maximum particle energy of 6 TeV. The 2015 beam test results were used to tune the energy response derived from MC simulations. Correction factors are 6.7% for $E_{T\,ASC} < 45$ GeV and 3.5% for $E_{T\,ASC} > 350$ GeV; the correction factor for intermediate energies was obtained using a linear interpolation [7]. The correction factor for helium nuclei can be found in Ref. [18]. The TASC crystals are subject to a phenomenon of light quenching for nuclei with a Z > 10, that is not reproduced by the MC simulations. This requires an *a posteriori* correction, obtained from the flight data, to the MC energy deposits generated in the TASC logs by noninteracting primary particles [21].

In order to obtain the flux measurement, energy unfolding is applied to correct E_{TASC} distributions for bin-to-bin migration effects, due to the limited energy resolution, and infer the primary particle energy. The response matrix is derived using MC simulation after applying the same selection procedure as for flight data. In all nuclei analyses, the Bayesian approach [30] implemented within the RooUnfold package [31] was used. The energy spectrum of each species is obtained from the unfolded energy distribution as follows:

$$\Phi(E) = \frac{N(E)}{\Delta(E)\epsilon(E)S\Omega T}$$

$$N(E) = U[N_{obs}(E_{TASC}) - N_{bg}(E_{TASC})]$$

where $S\Omega$ denotes the geometrical factor, T is the live time, E is the geometric mean of the lower and upper bounds of the bin, $\Delta(E)$ is the energy bin width, $N(E)$ identifies the bin content in the unfolded distribution, $\epsilon(E)$ is the total selection efficiency, $U()$ identifies the unfolding procedure operator, $N_{obs}(E_{TASC})$ denotes the bin content of observed energy distribution (including background), and $N_{bg}(E_{TASC})$ is the bin content of background events in the observed energy distribution.

For each flux used to compute the primary ratios a detailed assessment of the systematic contribution has been performed as explained in [7, 18–21]. The assessment of systematic errors on flux ratios is still under evaluation thus it is not reported here.

4. Results

The primary ratios between the iron (nickel) flux and the light element fluxes (carbon, oxygen
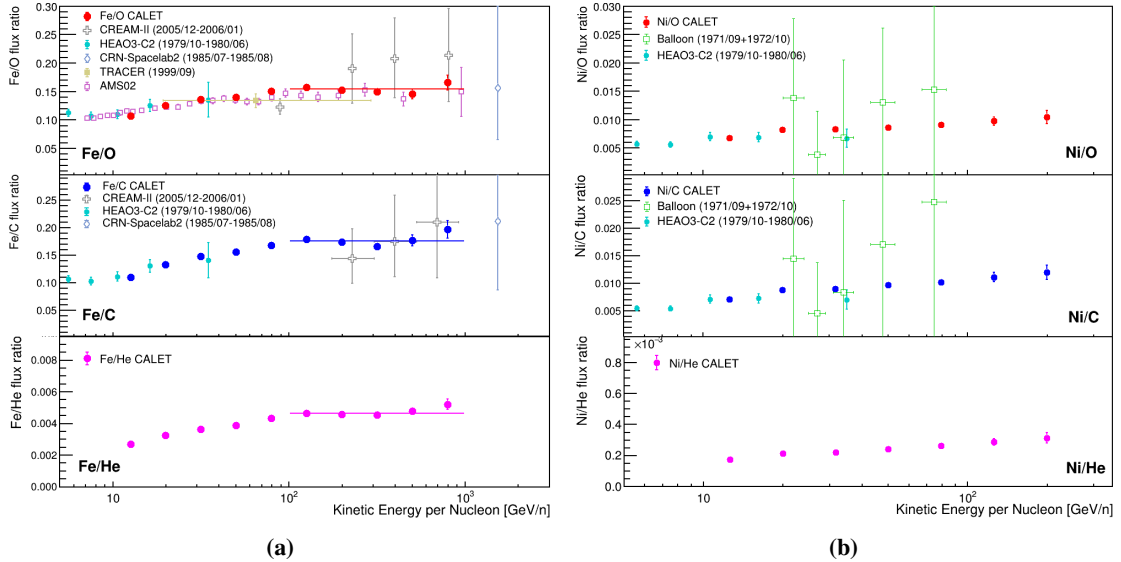

Figure 1: Measurement of the flux ratios (a) Fe/O, Fe/C and Fe/He and (b) Ni/O, Ni/C and Ni/He. CALET results are represented by the full colored circles and the error bars are representative of statistical uncertainty. In plot (a) the constant fit to the CALET results above 100 GeV/n is reported (see the main text for the results). Also plotted the measurement from HEAO3-C2 (cyan full squares), CREAM-II (gray open crosses), TRACER (mustard full squares), CRN (lilac open diamonds), HEN (green open squares).

and helium) are shown in fig. 1 where 5 bins per decades were used in all fluxes involved. The Fe/O, Fe/C and Fe/He flux ratios measured in the energy range between 12.5 GeV/n and 800 GeV/n are reported on the left panel of the figure together with a compilation of available measurements [1, 4, 32, 33]. CALET results are represented by the full colored dots and the errors bands are representative of statistical uncertainty. The Fe/O and Fe/C flux ratios agree well with the HEAO3-C2 [2] measurement at low energy and with CREAM-II [1] results in the high energy region. The Fe/O flux ratio is also compared with AMS02 [4], showing a good accordance both in shape and in normalization. No data are available in kinetic energy per nucleon for the comparison of the Fe/He flux ratio. These three ratios present a flat behavior above 100 GeV/n where a fit with a constant function gives Fe/O = 0.154 ± 0.002 with $\chi^2/dof = 4.1/4$, Fe/C = 0.176 ± 0.003 with a $\chi^2/dof = 5.7/4$ and Fe/He = $(4.64 ± 0.06) × 10^{-3}$ with $\chi^2/dof = 3.9/4$, confirming that C, O He and Fe have the same energy dependence above 100 GeV/n and thus suggesting a similar propagation mechanisms.
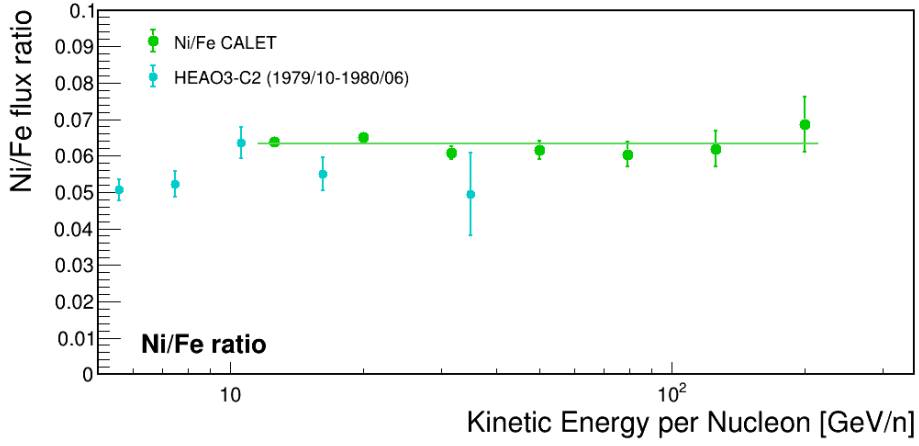

Figure 2: Nickel to iron flux ratio measured with CALET (green points). The errors bars are representative of statistical errors only. Data are fitted with a constant function giving Ni/Fe = 0.063 ± 0.001. Also plotted is the result from HEAO3-C2 [2].

The Ni/O, Ni/C and Ni/He flux ratios are reported in the right panel of Fig. 1 together with the few available measurements in the same energy interval [2, 9] extending the results up to ~ 200 GeV/n and improving the precision. The Ni/He ratio measured by CALET cannot be compared with other experimental results because there are not available measurements in the same energy range. The Ni/Fe flux ratio is reported in Fig. 2 and updates our previous result published in [20]. A 5 bins per decade binning has been used for these measurements. The Ni/Fe flux ratio is flat in all the energy region between 10 GeV/n and 200 GeV/n with a value of 0.063 ± 0.001 and a $\chi^2/dof = 5.4/6$ confirming that the spectral shape of Fe and Ni are the same within the experimental accuracy.

The ratio of light elements C/He, O/He (O/C) measured by CALET in the energy range between 12.5 GeV/n and 800 GeV/n (12.5 GeV/n and 1.9 TeV/n) is reported in fig. 3. The flat trend above 100 GeV/n is visible also in these cases and the fit with a constant function gives the following results: C/He = $(25.6 ± 0.2) × 10^{-3}$ with a $\chi^2/dof = 4.2/4$, O/He = $(29.2 ± 0.2) × 10^{-3}$ with a $\chi^2/dof = 9.6/4$, O/C = 1.14 ± 0.01 with a $\chi^2/dof = 5.04/5$. O/C can also be compared with

results from other experiments as reported in [7] showing a good accordance with HEAO3-C2 and AMS.
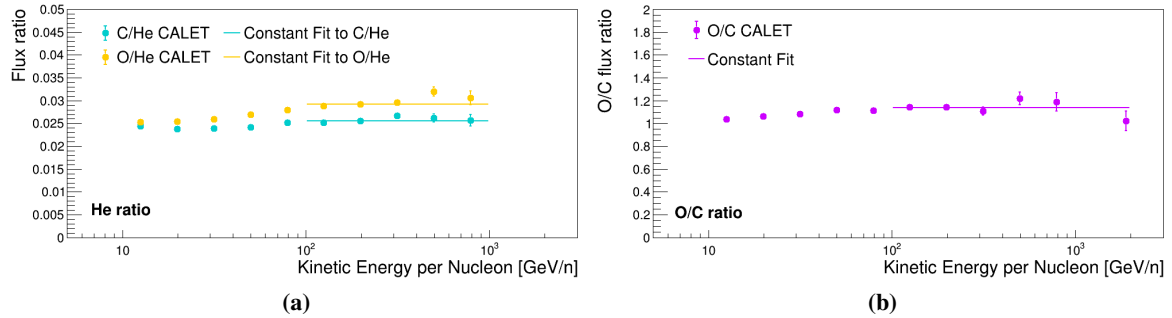

Figure 3: The flux ratios of light elements measured with CALET: (a) C/He (cyan fill circles) and O/He (yellow filled circles), (b) O/C (violet fill circles). The constant fit above 100 GeV/n is also reported (see the main text for the results).

Except for the Ni/Fe ratio, the behavior of all the other flux ratios below 100 GeV/n increases with the energy. For better comparison they have been normalized to the first point of the Ni/Fe ratio (the choice was arbitrary) and plotted together as can be seen in fig. 4. It is quite clear that in the region below 100 GeV/n Ni/O, Ni/C, Ni/He, Fe/O, Fe/C and Fe/He show a more pronounced increase compared to the behavior of Ni/Fe, O/He, C/He and O/C.

5. Conclusion

CALET on the International Space Station has measured the flux of several primary cosmic rays with a large sample of 7 years data to date. With the available data it was possible to compute the flux ratio of heavy elements (Fe and Ni) and light ones (He, C, O) and compare them with the ratio of light elements (O/He, C/He and O/C). It emerges that all the ratio are compatible with a
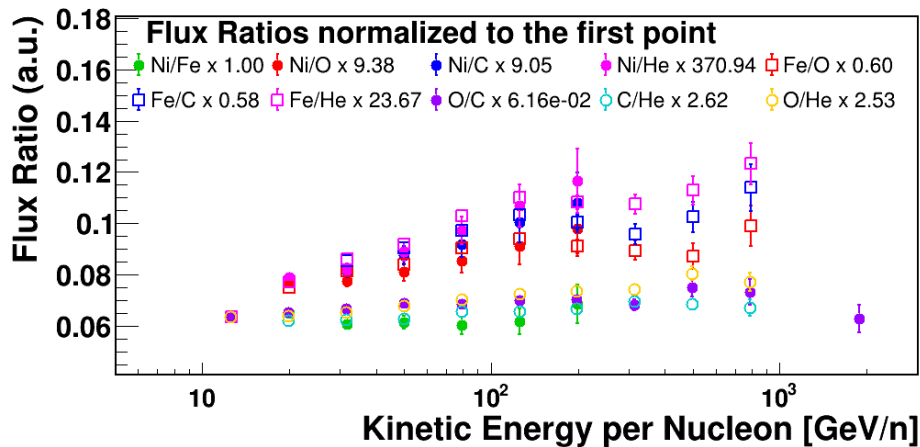

Figure 4: Comparison of CALET flux ratios: Ni/O (red points), Ni/C (blue points), Ni/He (magenta points), Fe/O (red squares), Fe/C (blue squares), Fe/He (magenta squares), O/C (violet points), C/He (cyan points) and O/He (yellow points) are normalized to the first point of Ni/Fe (green points).

constant above 100 GeV/n (Ni/Fe is constant starting from 10 GeV/n) whereas at low energy the ratio increases in a similar way for Ni/O, Ni/C, Ni/He, Fe/O, Fe/C, Fe/He. The increment at low energy is less pronounced for O/C, O/He and C/He.

Acknowledgments

References

[1] H.S. Ahn et al. *Astrophys. J.* **707** (2009) 593.

[2] J.J. Engelmann et al. *Astron. Astrophys.* **233** (1990) 96.

[3] M. Aguilar et al. *Phys. Rev. Lett.* **119** (2017) 251101.

[4] M. Aguilar et al. *Phys. Rev. Lett.* **126** (2021) 041104.

[5] M. Aguilar et al. *Phys. Rev. Lett.* **124** (2020) 211102.

[6] M. Aguilar et al. *Phys. Rev. Lett.* **115** (2015) 211101.

[7] O. Adriani et al. *Phys. Rev. Lett.* **125** (2020) 251102.

[8] G. Minagawa *Astrophys. J.* **248** (1981) 847.

[9] E. Juliusson *Astrophys. J.* **191** (1974) 331.

[10] A. Obermeier et al. *Astrophys. J.* **742** (2011) 14.

[11] S. Torii and P.S. Marrocchesi *Adv. Space Res.* **64** (2019) 2531.

[12] S. Torii in *Proceedings of Science (ICRC2017) 1092*, 2017.

[13] Y. Asaoka in *Proceedings of Science (ICRC2019) 001*, 2019.

[14] P. Marrocchesi in *Proceedings of Science (ICRC2021) 010*, 2021.

[15] O. Adriani et al. *Phys. Rev. Lett.* **119** (2017) 181101.

[16] O. Adriani et al. *Phys. Rev. Lett.* **120** (2018) 261102.

[17] O. Adriani et al. *Phys. Rev. Lett.* **129** (2022) 101102.

[18] O. Adriani et al. *Phys. Rev. Lett.* **130** (2023) 171002.

[19] O. Adriani et al. *Phys. Rev. Lett.* **129** (2022) 251103.

[20] O. Adriani et al. *Phys. Rev. Lett.* **128** (2022) 131103.

[21] O. Adriani et al. *Phys. Rev. Lett.* **126** (2021) 241101.

[22] K. Kasahara in *Proc. of 24th ICRC*, vol. 1, p. 399, 1995.

[23] T.T. Böhlen et al. *Nuclear Data Sheets* **120** (2014) 211.

[24] A. Ferrari et al. Tech. Rep. CERN-2005-10, INFN/TC_05/11, SLAC-R-773 (2005).

[25] J. Allison et al. *Nucl. Instrum. Methods Phys. Res., Sect. A* **835** (2016) 186.

[26] CALET collaboration *Astroparticle Physics* **100** (2018) 29.

[27] T. Niita et al. *Adv. Space Res.* **55** (2015) 2500.

[28] Y. Asaoka et al. *Astroparticle Physics* **91** (2017) 1.

[29] Y. Akaike in *Proceedings of Science (ICRC2015) 613*, 2015.

[30] G. D'Agostini *Nucl. Instr. and Meth. A* **362** (1995) 487.

[31] T. Adye in *Proc. of the PHYSTAT, CERN-2011-006*, 2011 [`arXiv:1105.1160`].

[32] D. Müller et al. *Astrophys. J.* **374** (1991) 356.

[33] F. Gahbauer et al., , *Astrophys. J.* **607** (2004) 333.

Full Author List: CALET Collaboration

O. Adriani[1,2], Y. Akaike[3,4], K. Asano[5], Y. Asaoka[5], E. Berti[2,6], G. Bigongiari[7,8], W.R. Binns[9], M. Bongi[1,2], P. Brogi[7,8], A. Bruno[10], N. Cannady[11,12,13], G. Castellini[6], C. Checchia[7,8], M.L. Cherry[14], G. Collazuol[15,16], G.A. de Nolfo[10], K. Ebisawa[17], A.W. Ficklin[14], H. Fuke[17], S. Gonzi[1,2,6], T.G. Guzik[14], T. Hams[11], K. Hibino[18], M. Ichimura[19], K. Ioka[20], W. Ishizaki[5], M.H. Israel[9], K. Kasahara[21], J. Kataoka[22], R. Kataoka[23], Y. Katayose[24], C. Kato[25], N. Kawanaka[20], Y. Kawakubo[14], K. Kobayashi[3,4], K. Kohri[26], H.S. Krawczynski[9], J.F. Krizmanic[12], P. Maestro[7,8], P.S. Marrocchesi[7,8], A.M. Messineo[8,27], J.W. Mitchell[12], S. Miyake[28], A.A. Moiseev[29,12,13], M. Mori[30], N. Mori[2], H.M. Motz[18], K. Munakata[25], S. Nakahira[17], J. Nishimura[17], S. Okuno[18], J.F. Ormes[31], S. Ozawa[32], L. Pacini[2,6], P. Papini[2], B.F. Rauch[9], S.B. Ricciarini[2,6], K. Sakai[11,12,13], T. Sakamoto[33], M. Sasaki[29,12,13], Y. Shimizu[18], A. Shiomi[34], P. Spillantini[1], F. Stolzi[7,8], S. Sugita[33], A. Sulaj[7,8], M. Takita[5], T. Tamura[18], T. Terasawa[5], S. Torii[3], Y. Tsunesada[35,36], Y. Uchihori[37], E. Vannuccini[2], J.P. Wefel[14], K. Yamaoka[38], S. Yanagita[39], A. Yoshida[33], K. Yoshida[21], and W.V. Zober[9]

[1]Department of Physics, University of Florence, Via Sansone, 1 - 50019, Sesto Fiorentino, Italy, [2]INFN Sezione di Firenze, Via Sansone, 1 - 50019, Sesto Fiorentino, Italy, [3]Waseda Research Institute for Science and Engineering, Waseda University, 17 Kikuicho, Shinjuku, Tokyo 162-0044, Japan, [4]JEM Utilization Center, Human Spaceflight Technology Directorate, Japan Aerospace Exploration Agency, 2-1-1 Sengen, Tsukuba, Ibaraki 305-8505, Japan, [5]Institute for Cosmic Ray Research, The University of Tokyo, 5-1-5 Kashiwa-no-Ha, Kashiwa, Chiba 277-8582, Japan, [6]Institute of Applied Physics (IFAC), National Research Council (CNR), Via Madonna del Piano, 10, 50019, Sesto Fiorentino, Italy, [7]Department of Physical Sciences, Earth and Environment, University of Siena, via Roma 56, 53100 Siena, Italy, [8]INFN Sezione di Pisa, Polo Fibonacci, Largo B. Pontecorvo, 3 - 56127 Pisa, Italy, [9]Department of Physics and McDonnell Center for the Space Sciences, Washington University, One Brookings Drive, St. Louis, Missouri 63130-4899, USA, [10]Heliospheric Physics Laboratory, NASA/GSFC, Greenbelt, Maryland 20771, USA, [11]Center for Space Sciences and Technology, University of Maryland, Baltimore County, 1000 Hilltop Circle, Baltimore, Maryland 21250, USA, [12]Astroparticle Physics Laboratory, NASA/GSFC, Greenbelt, Maryland 20771, USA, [13]Center for Research and Exploration in Space Sciences and Technology, NASA/GSFC, Greenbelt, Maryland 20771, USA, [14]Department of Physics and Astronomy, Louisiana State University, 202 Nicholson Hall, Baton Rouge, Louisiana 70803, USA, [15]Department of Physics and Astronomy, University of Padova, Via Marzolo, 8, 35131 Padova, Italy, [16]INFN Sezione di Padova, Via Marzolo, 8, 35131 Padova, Italy, [17]Institute of Space and Astronautical Science, Japan Aerospace Exploration Agency, 3-1-1 Yoshinodai, Chuo, Sagamihara, Kanagawa 252-5210, Japan, [18]Kanagawa University, 3-27-1 Rokkakubashi, Kanagawa, Yokohama, Kanagawa 221-8686, Japan, [19]Faculty of Science and Technology, Graduate School of Science and Technology, Hirosaki University, 3, Bunkyo, Hirosaki, Aomori 036-8561, Japan, [20]Yukawa Institute for Theoretical Physics, Kyoto University, Kitashirakawa Oiwake-cho, Sakyo-ku, Kyoto, 606-8502, Japan, [21]Department of Electronic Information Systems, Shibaura Institute of Technology, 307 Fukasaku, Minuma, Saitama 337-8570, Japan, [22]School of Advanced Science and Engineering, Waseda University, 3-4-1 Okubo, Shinjuku, Tokyo 169-8555, Japan, [23]National Institute of Polar Research, 10-3, Midori-cho, Tachikawa, Tokyo 190-8518, Japan, [24]Faculty of Engineering, Division of Intelligent Systems Engineering, Yokohama National University, 79-5 Tokiwadai, Hodogaya, Yokohama 240-8501, Japan, [25]Faculty of Science, Shinshu University, 3-1-1 Asahi, Matsumoto, Nagano 390-8621, Japan, [26]Institute of Particle and Nuclear Studies, High Energy Accelerator Research Organization, 1-1 Oho, Tsukuba, Ibaraki, 305-0801, Japan, [27]University of Pisa, Polo Fibonacci, Largo B. Pontecorvo, 3 - 56127 Pisa, Italy, [28]Department of Electrical and Electronic Systems Engineering, National Institute of Technology (KOSEN), Ibaraki College, 866 Nakane, Hitachinaka, Ibaraki 312-8508, Japan, [29]Department of Astronomy, University of Maryland, College Park, Maryland 20742, USA, [30]Department of Physical Sciences, College of Science and Engineering, Ritsumeikan University, Shiga 525-8577, Japan, [31]Department of Physics and Astronomy, University of Denver, Physics Building, Room 211, 2112 East Wesley Avenue, Denver, Colorado 80208-6900, USA, [32]Quantum ICT Advanced Development Center, National Institute of Information and Communications Technology, 4-2-1 Nukui-Kitamachi, Koganei, Tokyo 184-8795, Japan, [33]College of Science and Engineering, Department of Physics and Mathematics, Aoyama Gakuin University, 5-10-1 Fuchinobe, Chuo, Sagamihara, Kanagawa 252-5258, Japan, [34]College of Industrial Technology, Nihon University, 1-2-1 Izumi, Narashino, Chiba 275-8575, Japan, [35]Graduate School of Science, Osaka Metropolitan University, Sugimoto, Sumiyoshi, Osaka 558-8585, Japan, [36]Nambu Yoichiro Institute for Theoretical and Experimental Physics, Osaka Metropolitan University, Sugimoto, Sumiyoshi, Osaka 558-8585, Japan, [37]National Institutes for Quantum and Radiation Science and Technology, 4-9-1 Anagawa, Inage, Chiba 263-8555, Japan, [38]Nagoya University, Furo, Chikusa, Nagoya 464-8601, Japan, [39]College of Science, Ibaraki University, 2-1-1 Bunkyo, Mito, Ibaraki 310-8512, Japan